Original Article

JCBFM

Journal of Cerebral Blood Flow & Metabolism
0(0) 1–13

DOI: 10.1177/0271678X231191600
journals.sagepub.com/home/jcbfm
Sage

Brain-wide continuous functional ultrasound imaging for real-time monitoring of hemodynamics during ischemic stroke

Clément Brunner[1,2,3,4], Nielsen Lagumersindez Denis[5,6,7], Karen Gertz[5,6,7], Micheline Grillet[1,2,3,4], Gabriel Montaldo[1,2,3,4], Matthias Endres[5,6,7] and Alan Urban[1,2,3,4]

Abstract

Ischemic stroke occurs abruptly causing sudden neurologic deficits, and therefore, very little is known about hemodynamic perturbations in the brain immediately after stroke onset. Here, functional ultrasound imaging was used to monitor variations in relative cerebral blood volume (rCBV) compared to baseline. rCBV levels were analyzed brain-wide and continuously at high spatiotemporal resolution (100 μm, 2 Hz) until 70mins after stroke onset in rats. We compared two stroke models, with either a permanent occlusion of the middle cerebral artery (MCAo) or a tandem occlusion of both the common carotid and middle cerebral arteries (CCAo + MCAo). We observed a typical hemodynamic pattern, including a quick drop of the rCBV after MCAo, followed by spontaneous reperfusion of several brain regions located in the vicinity of the ischemic core. The severity and location of the ischemia were variable within groups. On average, the severity of the ischemia was in good agreement with the lesion volume (24 hrs after stroke) for MCAo group, while larger for the CCAo + MCAo model. For both groups, we observed that infarcts extended to initially non-ischemic regions located rostrally to the ischemic core. These regions strongly colocalize with the origin of transient hemodynamic events associated with spreading depolarizations.

Keywords

Brain-wide imaging, functional ultrasound imaging, ischemic lesion prediction, ischemic stroke, spreading depolarization

Received 7 June 2023; Revised 13 July 2023; Accepted 14 July 2023

Introduction

Acute ischemic stroke is most often caused by occlusion of a cerebral artery. It is characterized by a sudden loss of blood circulation to an area of the brain, resulting in a corresponding loss of neurologic function. Ischemic stroke triggers a decrease of blood supply in the affected tissue which is timely key when considering the tissue fate.[1–3] Hemodynamics and characteristics of lesion growth following immediately after vessel occlusion are essential issues and represent a new target area for promising therapeutic interventions.

However, imaging hemodynamics immediately after the stroke onset at the brain-wide scale remains difficult to achieve, even in preclinical investigation. Indeed, most of conventional modalities suited for whole-brain imaging (MRI, PET, SPECT)[4,5] have limited spatial and/or temporal resolution to resolve vascular responses dynamically. On the other hand, neuroimaging techniques with high resolution capacities and well suited to capture hemodynamics (LDF, LSCI, OIS, 2PM, PAM)[6,7] are constrained by a reduced

[1]Neuro-Electronics Research Flanders, Leuven, Belgium
[2]Vlaams Instituut voor Biotechnologie, Leuven, Belgium
[3]Interuniversity Microelectronics Centre, Leuven, Belgium
[4]Department of Neurosciences, KU Leuven, Leuven, Belgium
[5]Department of Neurology and Center for Stroke Research Berlin, Charité-Universitätsmedizin, Berlin, Germany
[6]German Center for Neurodegenerative Diseases (DZNE), Berlin, Germany
[7]German Centre for Cardiovascular Research (DZHK), Berlin, Germany

Corresponding author:
Alan Urban, Neuro-Electronics Research Flanders, 3001 Leuven, Belgium.
Email: alan.urban@nerf.be

field-of-view (e.g., brain surface, limited depth of field). While combining multi-modal neuroimaging strategies would provide key insights, real-time and brain-wide imaging of stroke hemodynamics remains challenging. Functional ultrasound imaging has been successful for brain imaging of evoked activity which are transient hemodynamic events[8,9] or epileptiform seizures in rodent brain.[9] Indeed, this modality measures local changes in cerebral blood volume (CBV) with a spatial resolution of $\sim 100 \times 300 \times 100\,\mu m^3$, a temporal resolution of $\sim$0.1 s, and down to 1.5-cm depth, enough to image the entire rodent brain depth.[9–11] Therefore, functional ultrasound imaging is well suited for preclinical stroke research. Hence, it has been successfully employed to study i) chronic brain-wide perfusion changes after transient intraluminal occlusion of the middle cerebral artery (MCAo),[12] ii) post-ischemic and post-recanalization reorganization of brain functions after distal MCAo,[13] and iii) brain-wide imaging of stroke perfusion after thromboembolic stroke and recanalization.[14]

However, these studies focused mainly on the ischemic core and do not describe in detail the hemodynamic changes in the peri-ischemic tissue. Indeed, spreading depolarization (SD), a slowly propagating wave of intense depolarization travelling across the cortical tissue coupled with transient and local changes in cerebral perfusion,[15,16] has been described to potentially exacerbate ischemic injury.[17–22] While the features of SDs induced by ischemia have been widely examined, studies generally failed to identify their site of elicitation. Therefore, precise tracking of the stroke hemodynamics i.e., ischemia and SDs, at the brain-wide scale could help to better understand their impact on pathophysiology.

In this study, we used functional ultrasound imaging to monitor real-time hemodynamics during stroke, including perfusion and peri-ischemic SDs at the brain-wide scale. We compared two rat stroke models, i.e., a first model consisting of permanent occlusion of the distal branch of the middle cerebral artery (MCAo) resulting in small ischemic lesions and a second model with a tandem occlusion of the common carotid and middle cerebral arteries (CCAo + MCAo) resulting in larger and more robust ischemic lesions.[23–25] Hemodynamic changes were monitored continuously until 70 mins after stroke onset. Data were then registered, segmented, and clustered[26,27] into 115 anatomical regions, including cortical, thalamic, striatal, and hippocampal areas using a digitalized rat brain atlas based on Paxinos.[28] Comparing the ischemic territory and the infarcted tissue at 24 hrs revealed a mismatch for both size and location for both stroke models. Notably, we observed that brain regions located rostrally of the ischemic core are not affected by the ischemia up to 70 mins after stroke but became part of the ischemic lesion within the 24 hrs post-stroke. These regions are also from where SDs emerge quickly after the stroke onset.

Material and methods

Animals

Experimental procedures were approved by the Committee on Animal Care of the Catholic University of Leuven, in accordance with the national guidelines on the use of laboratory animals and the European Union Directive for animal experiments (2010/63/EU). The manuscript was written according to the ARRIVE Essential 10 checklist for reporting animal experiments.[29] Adult male Sprague-Dawley rats (n = 24; Janvier Labs, France) were housed in standard ventilated cages and kept in a 12:12 hrs reverse dark/light cycle environment at a temperature of 22°C with *ad libitum* access to food and water. To avoid selection bias, animals were randomly distributed in three experimental groups: (i) MCAo, in which the distal branch of the left MCA was permanently occluded (n = 10; 289.8 ± 51.7 g), (ii) CCAo + MCAo, in which the left CCA was permanently occluded shortly before the MCAo (n = 10; 278.4 ± 40.2 g), (iii) a sham group where four rats (252.5 ± 15.2 g) were imaged as in any other group, but the microvascular clip was inserted next to the MCA without occluding it. Note that one experimenter (C.B.) performed the entire procedure, from skull opening, vessel occlusion to brain imaging, for all animals of the study.

Cranial window for brain-wide imaging

A cranial window was performed in all rats under isoflurane anesthesia (Iso-Vet, Dechra, Belgium) continuously delivered at 0.6 l/min through a nose mask. A mixture of 5% isoflurane in compressed dry air was used to induce anesthesia, subsequently reduced to 2.0–2.5% during surgery and to 1.5% for imaging. From surgery to the end of the imaging session, the animal head was fixed and secured on a stereotaxic frame with all nose clamp and ear bars (Rat Standard Stereotaxic 51601, Stoelting Co., USA). Body temperature was monitored using a rectal probe and maintained at 36.5 ± 0.5°C using a digitally controlled heating blanket (CODA, Kent Scientific Corp., USA). Intraperitoneal injection of 5% glucose solution was provided every 2 hrs to prevent dehydration. As preoperative analgesia, Xylocaine (0.5%, AstraZeneca, England) was injected subcutaneously into the head skin. The scalp was shaved and cleaned with isobetadine before removing the entire dorsal skull.

The cranial window extended from bregma (ß) +4.0 to −7.0 mm anterior to posterior, laterally 6.0 mm to the right side, until the parietal-squamosal suture on the left side to expose the distal branch of the MCA was performed as previously described.[8,12,13] Sterile saline was regularly added during drilling sessions to avoid overheating the tissue. The skull was carefully removed without damaging the dura. Finally, the brain was covered with a low-melting 2% agarose (Sigma-Aldrich, USA) and ultrasound gel (Aquasonic Clear, Parker Laboratories Inc, USA) to ensure a proper acoustic coupling with the ultrasound probe.

MCAo and CCAo + MCAo procedures

Rats from the CCAo + MCAo group underwent CCA dissection before cranial window surgery. Briefly, the rat was placed in a supine position to shave and clean neck hairs. A vertical incision was made on the neck, and the left CCA was carefully dissected from the surrounding tissue and exposed, avoiding damaging the vagus nerve.[23,30] A 3-0 surgical silk thread (Ethicon, France) was placed around the CCA and remained untightened until occlusion during the imaging session. Rats from MCAo and CCAo + MCAo groups were subjected to a permanent MCA occlusion directly during the imaging session using a microvascular clip (#18055-03, micro-serrefine, FST GmbH, Germany) that was manually refined by grinding for optimal serration of the MCAo in adult rats.

Functional ultrasound imaging

The data acquisition was performed using a functional ultrasound imaging scanner equipped with custom acquisition and processing software described by Brunner, Grillet et al.[27] In short, the scanner is composed of a linear ultrasonic transducer (15 MHz, 128 elements, Xtech15, Vermon, France) connected to 128-channel emission-reception electronics (Vantage, Verasonics, USA) that are both controlled by a high-performance computing workstation (fUSI-2, AUTC, Estonia). The ultrasound transducer was secured using a custom-design 3D printed transducer holder and translated over the rat head using a linear motor stage (T-LSM200A, Zaber Technologies Inc., Canada) controlled by the imaging workstation, thus allowing for robust and repetitive anteroposterior scanning of the brain (details about 3D printed pieces, setup, and synchronization of imaging with motor translation can be found in Brunner, Grillet et al.[27] and open-access[31]) Imaging is performed on an anti-vibration table to minimize external sources of vibration. Each coronal Doppler image is 12.8-mm width and 9-mm depth and comprises 300 compound images acquired at 500 Hz. Each compound image is computed by adding nine plane-wave (4.5 kHz) angles from −12° to 12° with a 3° step. The blood signal was extracted from 300 compound images using a single value decomposition filter and removing the 30 first singular vectors.[32] The Doppler image is computed as the mean intensity of the blood signal in these 300 frames that is an estimator of the cerebral blood volume (CBV).[9,10] This sequence enables a temporal resolution of 0.6 s, an in-plane resolution of 100 × 110 µm, and an off-plane (thickness of the image) of 300 µm.[27]

2D scan of brain vasculature

Before occlusion, we performed a high-resolution 2D scan of the brain vasculature consisting of 89 coronal planes from bregma (ß) +4.0 to −7.0 mm spaced by 125 µm. This scan was used for data registration. During the 90-min imaging session, the same brain area was scanned at lower resolution with only 23 planes with a step of 500 µm that took approximately 23 s to complete. The number of imaging planes was chosen to maximize the number of brain volumes scanned per min while preserving a good resolution in the anteroposterior axis. For the MCAo group, a 20-min baseline was recorded before occluding the MCA, whereas the CCAo + MCAo group has a 10-min baseline before CCAo, followed by the MCAo 10mins later. Notably, the procedures were performed live with a real-time display of the Doppler images, allowing for monitoring the brain perfusion and the direct confirmation of the CCA and/or MCA occlusions (Movies 1 to 3 – Artifactual signal driven by air bubbles trapped in the ultrasound gel is addressed in Supplementary Figure 2). The imaging session was stopped after 90 mins of recording. At the end of the imaging section, the neck skin was sutured with a 2-0 surgical silk thread (Ethicon, France) and Metacam (0.2 mg/kg, Boehringer Ingelheim, Canada) was injected subcutaneously for postoperative analgesia, and rats were placed in a warm cage and monitored until waking up.

Registration and segmentation

We developed a custom digital rat brain atlas for registration of the data based on the one stereotaxic atlas of Paxinos.[28] The spatial transformation matrix was computed on the high-resolution 2D scan that was manually aligned on the atlas following the procedure described in Brunner, Grillet et al.[27] In short, the high-resolution 2D scan of the brain vasculature was translated and rotated to align the 2D scan of the rat brain to a digital version of the rat Paxinos atlas.[28] For an accurate registration, we used landmarks such as the

surface of the brain, ventricles, hippocampus, superior sagittal sinus, and other large vessels. If needed, the brain volume was scaled to fit the atlas outline. Then, the registration was refined by adjusting the position of the volume using brain landmarks such as lateral ventricles, hippocampus, and large vessels. The outcome of this registration procedure is an affine coordinate transformation: $\vec{r} = M\vec{r} + \vec{a}$, where $\vec{r} = (x, y, z)$ are the original coordinates of high-resolution 2D scan of the brain vasculature, M is the rotation and scaling matrix and $\vec{a}$ the translation vector. Finally, this affine transformation was applied to the low-resolution 2D scan with the same axis origin as the high-resolution 2D scan. The registration was performed in a blinded fashion by two different operators, and we verified that both results were consistent. The dataset was segmented into 115 anatomical regions/hemispheres that were subsampled from the 332 brain regions of the original atlas (see Supplementary Table 1). The hemodynamic signals were averaged in each area. The transformation of the low-resolution 2D scan and the data processing of 2D scan was performed using an automated MatLab-based pipeline. The software for data registration and segmentation is open-access here.[33] The unrolled-cortex representation corresponds to the maximum intensity projection of the signal located 250 µm under the cortical surface (see Supplementary Figure 1).

Relative cerebral blood volume (rCBV)

We used the relative cerebral blood volume (rCBV; expressed in % compared to baseline) to analyze ischemia defined as the signal in each voxel compared to its average level during the baseline period (Figure 1). After registration and segmentation, the rCBV signal was averaged in each individual region.

Clustering of the rCBV loss

Once registered and segmented, the brain regions were clustered based on the average rCBV loss after the MCA occlusion and sorted from the most significant loss of rCBV signal to the smallest (from 1 to 115) as compared to baseline level. The list of the brain regions clustered can be found in Supplementary Table 1.

Analysis of spreading depolarizations

The detection of spreading depolarizations (SDs) was performed based on the temporal analysis of the rCBV signal. The rCBV signal was averaged in an area of interest (10×10 voxels) located in the left side cortex, laterally to the ischemic territory. An SD is defined as a transient increase of rCBV signal above 50% compared to baseline. This procedure allowed to measure the occurrence of SDs over the recording period and their propagation pattern in the field of view. The velocity of each SDs was calculated as the time spent to propagate between two areas of interest located in the left side cortex, along with the ischemic territory. The origin of each SDs was located by tracking back the trajectory to the region of the first detection of the transient increase of rCBV. The occurrence, the propagation pattern, and the velocity of SDs could be efficiently visualized using the unrolled-cortex projection as presented in Movie 3.

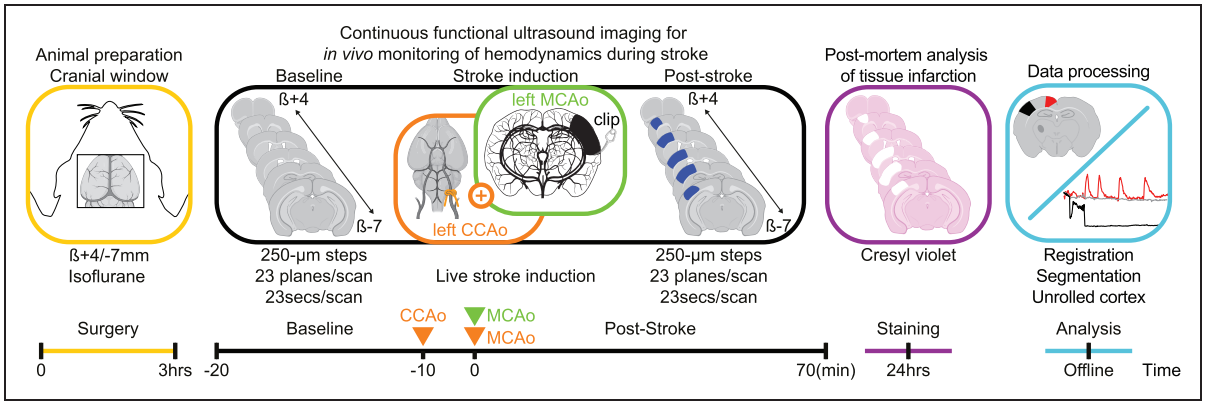

Figure 1. Experimental workflow and timeline. From left to right. An 11 × 13-mm cranial window was performed to access the whole brain by functional ultrasound imaging before occluding the middle cerebral artery occlusion (MCAo) or MCAo combined with the common carotid artery (CCAo + MCAo). Image acquisition has been performed continuously for 90 mins by scanning the brain repeatedly in the anteroposterior direction (23 secs/scan) before, during, and after stroke onset. After the experiments, rats returned to their home cage and were euthanized 24 hrs after occlusion to quantify the infarct size using cresyl violet staining. We developed a digital version of the rat Paxinos atlas[28] for the registration, segmentation, and temporal analysis of ischemia using a dedicated software solution.[33]

Histopathology

Rats were killed 24 hrs after the occlusion for histological analysis of the infarcted tissue. Rats received a lethal injection of pentobarbital (100 mg/kg i.p. Dolethal, Vetoquinol, France). Using a peristaltic pump, they were transcardially perfused with phosphate-buffered saline followed by 4% paraformaldehyde (Sigma-Aldrich, USA). Brains were collected and post-fixed overnight. 50-µm thick coronal brain sections across the MCA territory were sliced on a vibratome (VT1000S, Leica Microsystems, Germany) and analyzed using the cresyl violet (Electron Microscopy Sciences, USA) staining procedure. Slices were mounted with DPX mounting medium (Sigma-Aldrich, USA) and scanned using a brightfield microscope. Ischemic lesion areas were manually delineated and measured by two researchers independently in double-blind conditions using the Fiji software.[34] Brain slices were then registered on the rat atlas utilizing a set of landmarks, including the overall size of the slice, the cortical thickness, the positions of ventricles, and the position/size of the hippocampus. The ischemic lesion was projected in the unroll-cortex using the same approach as defined previously (see above and Supplementary Figure 1).

Statistical analysis

The dataset successfully passed Shapiro-Wilk and Kolmogorov-Smirnov tests (significance level $\alpha = 0.05$) for normal distribution before being subjected to statistical analysis, see details in results and figure captions. All data are shown as mean±sd (standard deviation). Statistical analysis were performed using Prism9.3.1 (GraphPad Software).

Results

Animals

Three rats from the MCAo group were excluded from the analysis because we observed an extensive *postmortem* hemorrhage extending in the cortex and subcortical regions. It was probably caused by a displacement of the microvascular clip during the 24 hrs recovery period. Therefore, the number of rats in this group was reduced to $n = 7$ for the analysis.

Brain-wide continuous monitoring of hemodynamics

The functional ultrasound imaging scanner allows repeated 2D scans in the anteroposterior direction. For the first time, we demonstrate the applicability of this technology for large-scale and continuous monitoring of hemodynamics in deep brain tissue before, during, and after stroke onset. After data acquisition, every 23 cross-sections spaced of 500 µm were registered and segmented on a custom-developed digital rat atlas (see Materials and Methods) to provide a volumetric and dynamic view of the changes in perfusion at high spatiotemporal resolution.

Typical plots of the temporal evolution of the hemodynamic signal are shown in Figure 2(a) for both the MCAo (green plot) and CCAo + MCAo (orange plot) stroke models. In this example, the variations in the cerebral perfusion were measured as rCBV compared to the baseline level in two regions of interest located either in the ischemic core in the left hemisphere (S1BF) or in the opposite control hemisphere (black ROI and plots). As shown, for the MCAo stroke model (Figure 2(a), green plot), the rCBV signal dropped immediately by ∼−50% after MCAo and remained around this value during the entire duration of the experiment. On the contrary, we observed a two-step and a more profound decrease of the rCBV signal (Figure 2(a), orange line) in the CCAo + MCAo stroke model. First, we observed a transient drop of the rCBV to approximately −60% of the baseline level caused by the CCA occlusion that quickly recovered but not up to the initial values. Then, the MCAo triggers a massive reduction of ∼−95% of the rCBV that remains at this level during the entire recording. Interestingly, in the CCAo + MCAo stroke model, the contralesional hemisphere also shows a transient drop of ∼−15–20% of the rCBV signal after CCAo that is not exacerbated after MCAo (Figure 2(a), black line). Note that the rCBV in the control ROI located in the opposite hemisphere remains stable all along with the experiment in both stroke models (Figure 2(a), dark line).

Figure 2(b) provides a detailed view of hemodynamic changes in 115 brain regions in the affected hemisphere (See Supplementary Table 1) averaged for all animals in each group (MCAo group, $n = 7$; CCAo + MCAo group, $n = 10$). Each region is sorted from the most significant loss of rCBV signal to the smallest (from 1 to 115).

Four levels of rCBV loss when compared to baseline level (−100% to −60%; −60% to −40%, −40% to −20%, and −20% to 0%) were defined to better compare the MCAo and CCAo + MCAo stroke models. At rCBV loss comprised between −100% to −60%, we noticed that more regions were affected in the CCAo + MCAo than in the MCAo stroke model (∼20 vs. ∼10, respectively), confirming the cumulative effect of MCAo + CCAo on the reduction of the perfusion. All these regions were exclusively located in the cortex. For rCBV loss ranging between −60% and −40%, approximately the same number of regions (∼30) were affected in the two models, but we observed

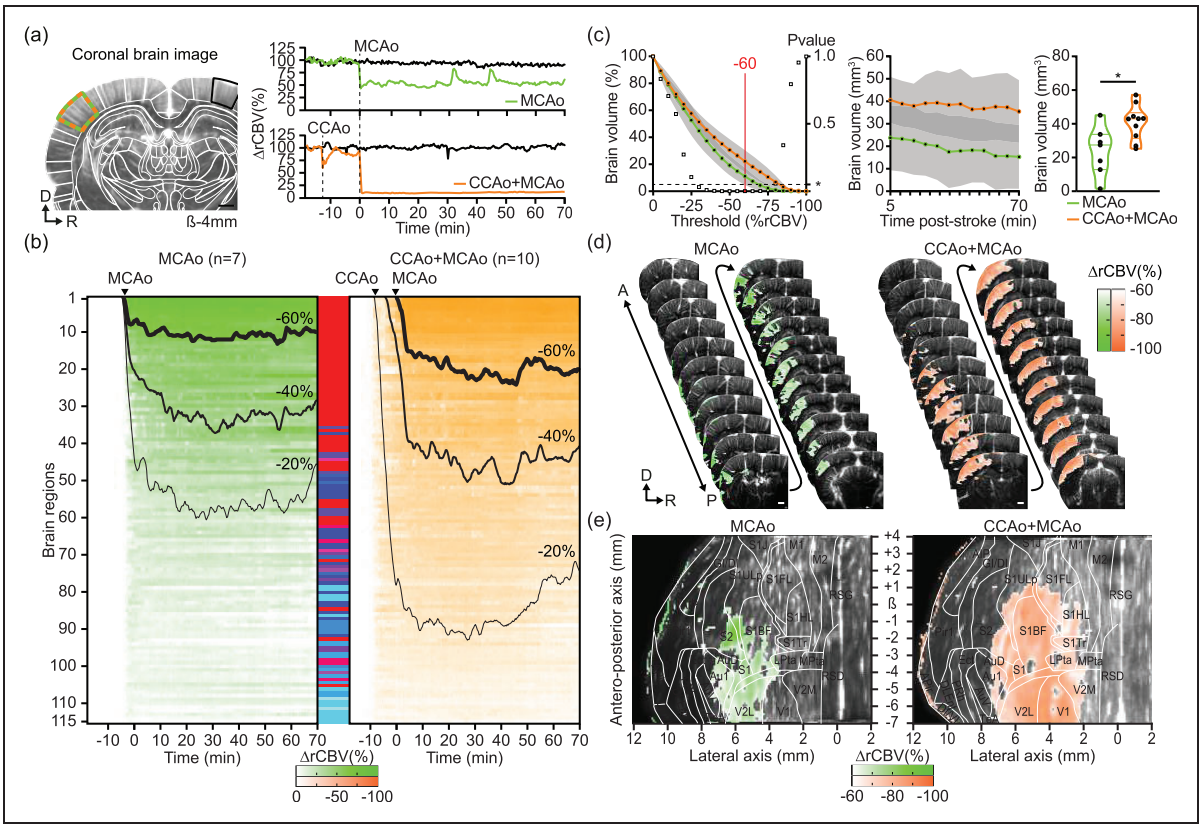

Figure 2. Brain-wide continuous and real-time monitoring of hemodynamics during ischemic stroke. (a) A typical image of the brain microvasculature for one coronal cross-section from the 2 D scan before the stroke. Only the left hemisphere is imaged entirely here because of the too-small size of the ultrasound transducer used for this study. All images were registered and segmented based on a digital version of the rat Paxinos atlas[28] (white outlines). Time series plots of the average signal in the primary somatosensory barrel-field cortex (S1BF; green and orange region) in the affected hemisphere and the control ROI located in the opposite hemisphere (black region) for each stroke model (MCAo in green; CCAo + MCAo in orange). (b) Global hemodynamic changes (rCBV) in 115 regions located in the ischemic hemisphere for both the MCAo (left and green panel) and CCAo + MCAo groups (right and orange panel). Regions were clustered according to the extent of rCBV signal loss (from more to less pronounced; find red-to-blue color-coded labels in Supplementary Table 1). (c) Left to right. Plot showing the total volume of brain region corresponding to a given rCBV decrease (%; mean ± sd) and associated statistical difference (P-value, black square Unpaired t-test, *$p < 0.05$; left panel) between ischemic territory volumes in the MCAo (green, n = 7) and CCAo + MCAo groups (orange, n = 10). (d) Typical 2D brain scan of hemodynamics showing the loss in rCBV induced by either MCAo (left panel) or CCAo + MCAo (right panel). 22 cross-sections out of 23 are represented here. (e) Unrolled-cortex projection (see Supplementary Figure 1) showing the loss in rCBV induced by either MCAo (left panel) or CCAo + MCAo (right panel). D: dorsal, R: right, A: anterior, P: posterior, ß: Bregma reference point. Scale bars: 100 µm.

that those regions tend to be slightly reperfused naturally over time (Figure 2(b)). Furthermore, we identified 50–60 regions located in the cortex with a drop of rCBV between −40% to −20% of the baseline level in the MCAo group, whereas 80–90 regions were affected for the same levels in the MCAo + CCAo group also including subcortical structures (Figure 2(b) and Supplementary Table 1).

To evaluate the relevance of the rCBV signal to precisely assess the perfusion status and differentiate each stroke model, we quantified the affected brain volume (in mm^3) for various levels of rCBV decrease (Figure 2(c)). We observed that ischemic volume differs significantly (P-value, black square Unpaired t-test, *$p < 0.05$) between the MCAo and the CCAo + MCAo groups for values ranging from −30 to −75% (Figure 2(c)), left panel; mean ± sd). The most significant difference between the two groups was observed for the value −60% that was chosen for further analysis (Figure 2(c) to (e)).

The total volume of brain tissue showing an rCBV reduction of −60% was then analyzed during the entire imaging session. We observed that the volume of ischemic tissue for the CCAo + MCAo group was 41 ± 10 mm^3 and did not show a significant change between the MCA occlusion and the end of the imaging period (35 ± 14 mm^3; Figure 2(c), middle panel; mean ± sd; $p > 0.44$, GLM-based repeated measures

one-way ANOVA). On the contrary, the volume of tissue affected for the MCAo group tends to shrink over time from $24 \pm 14\,mm^3$ quickly after MCAo to $15 \pm 14\,mm^3$ after 70 mins afterward (Figure 2(c), middle panel; mean ± sd; $p < 0.0001$, GLM-based repeated measures one-way ANOVA). Interestingly, the differences between the two groups for an rCBV level of −60% were already statistically significantly different at 5mins after stroke onset. It became even more pronounced during the 70 mins imaging period (Figure 2(c), right panel; $p = 0.013$; Unpaired t-test).

Figure 2(d) presents a typical case for each model in which we overlaid the ischemic territory on top of each microvascular image collected during brain scans for each stroke model. We projected and unrolled the cortical regions into a flat surface overlaid with the anatomical landmarks from the reference rat brain atlas to appreciate the differences better. Such a view is advantageous for accurately visualizing the regions with reduced rCBV, their spatial extent (Figure 2(e) and Supplementary Figure 1) and comparing animals and models.

A large part of the infarct is located in regions not ischemic at 70mins after stroke onset

Cresyl violet staining of coronal brain slices was performed 24 hrs after the experiments. A typical example is presented in Figure 3(a). It shows that the infarcted area is localized only in the cortex in both stroke models, but MCAo caused a much smaller and less extensive lesion (Figure 3(a), left panel; green area) than CCAo + MCAo (Figure 3(a), right panel; orange area).

The statistical analysis of all rats confirmed that the infarct volume is significantly larger for the CCAo + MCAo group ($75 \pm 28 mm^3$, range [26.62–123.26], $n = 10$, mean ± sd; Figure 3(b), in orange) when compared to the MCAo group ($24 \pm 10\,mm^3$, range [2.92–33.17], $n = 7$, mean ± sd; Figure 3(b), in green; ***$p = 0.0003$, unpaired t-test). Note that these results agree with rCBV data, also showing a larger ischemic territory in the CCAo + MCAo group. Taken together, this demonstrates that functional ultrasound images acquired at early time points after stroke onset (from 5 to 70 mins) have an excellent predictive value to predict brain infarction. To confirm this hypothesis, we compared the results obtained by histopathology with those from functional ultrasound imaging in each stroke model that were both presented using the same unrolled-cortex projection as described previously (see Supplementary Figure 1). Figure 3(c) shows a typical case for each group. We observed in the MCAo model (Figure 3(c), left panel) that the infarcted region (green outline) only partially coincides with regions showing reduced rCBV (green shading). Interestingly, much of the infarcted tissue is located rostrally to the region with low rCBV at 70 mins, in an area that was not initially ischemic. On the contrary, we observed a considerable overlap between the infarct region and the initially ischemic region at 70 mins in the CCAo + MCAo model (Figure 3(c), right panel) even though, here again, non-overlapping regions were observed in the anterior part of the brain. Nevertheless, when total infarct size was compared with the initial ischemic territory, it was preserved in the MCAo but not in the CCAo + MCAo model, in which the infarct volume was much smaller than the initial ischemic region.

Although we observed large variability in terms of the location and size of the infarct at 24 hrs after stroke compared with the ischemic areas at 70 mins after stroke onset for each animal (Figure 3), these results were confirmed at the group level, showing that the infarcted territory extends rostrally to the ischemic region by 1.53 ± 1.68 and 1.37 ± 0.66 mm, respectively in MCAo and CCAo + MCAo groups ($p = 0.49$, Unpaired t-test). This mismatch is consistent for the two groups (6/7 for MCAo and 7/7 for CCAo + MCAo rats). Additionally, we noticed that the MCAo group also shows, on average, a mismatch between the position of the infarct and the areas of low rCBV in the posterior part of the brain, where we previously observed good reperfusion during the 70-min period of the functional ultrasound imaging recording (Figure 2(b) and (c)). In both groups, these results indicate that the lack of blood supply may not be the only factor contributing to the infarction of the brain.

These findings prompted us to evaluate other important factors, such as SDs that have been shown to exacerbate focal ischemic injury by converting zones of the viable but non-functional ischemic penumbra to the core region beyond rescue.[35]

Spreading depolarizations start quickly after MCAo

As shown in previous studies, functional ultrasound imaging is suitable for whole-brain tracking of transient hyperemic events associated with SDs.[9,36] The imaging protocol that we developed for this study allows for detection, monitoring, and quantification of SDs in real-time before, during, and after stroke onset. The spatiotemporal profile of SDs was extracted by averaging the rCBV signal in all voxels from the retrosplenial granular cortex (RSG) that is located in the vicinity of the region with the low level of rCBV (Figure 4(a), left panel). As already observed in previous studies, SDs were triggering transient hyperemia characterized by a rapid and massive increase of the rCBV signal (>+150% rCBV), often followed by a sustained reduction of the baseline level. Recorded SDs

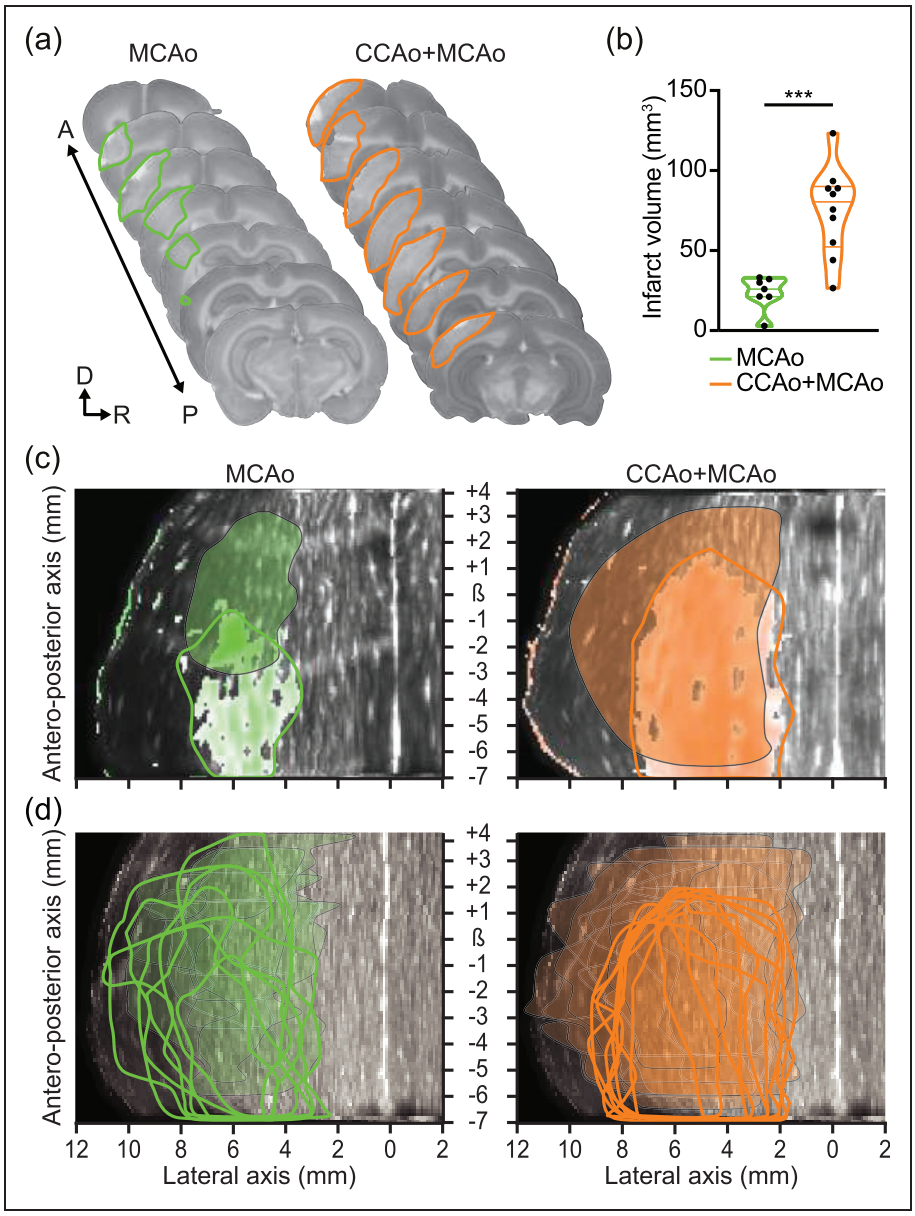

Figure 3. Size and location of the region with a low rCBV signal at 70mins do partially overlap with the infarct at 24 hrs. (a) Typical rat brain cross-section stained by cresyl violet to evaluate the infarct size at 24 hrs after MCAo (left) or CCAo + MCAo (right). The infarcted territory is highlighted for each stroke model (green and orange, respectively). (b) Comparison of the infarct volume (mm^3) between the two models, showing the CCAo + MCAo (orange) display a statistically more extensive infarct than the MCAo group (green; Unpaired t-test, ***$p = 0.0003$). (c) The infarct (colored shadings) and the region with low rCBV levels (colored outlines) are overlaid on the unrolled-cortex projection for one typical rat. (d) Same as in (c) but for all rats used in the study. D: dorsal, R: right, A: anterior, P: posterior, ß: Bregma reference point.

show some variance in hyperperfusion pattern (amplitude, duration, shape) while early and transient hypoperfusion drop was detected in just few SDs (Figure 4(a), right panel; Movies 2 and 3; Supplementary Figure 3). We did not observe a significant difference in the number (4.3 ± 2.3 and 4.7 ± 2.9, mean ± sd, $p = 0.7557$, Unpaired t-test) and the frequency (1 SD each 17.5 mins and 15.2 mins, central frequency) of SDs between the MCAo and CCAo + MCAo groups (Figure 4(b)). A detailed analysis of one individual animal revealed that all SDs are generated within the same brain region (Movie 3). Moreover, SDs were mainly detected within the same brain region, where rCBV loss was ~50% (see Supplementary Figure 4). The sham-operated rats ($n = 4$) had a maximum of one SD with distinct and transient hyperemia propagating over the cortex followed by a long-lasting oligemia observed along the recording period

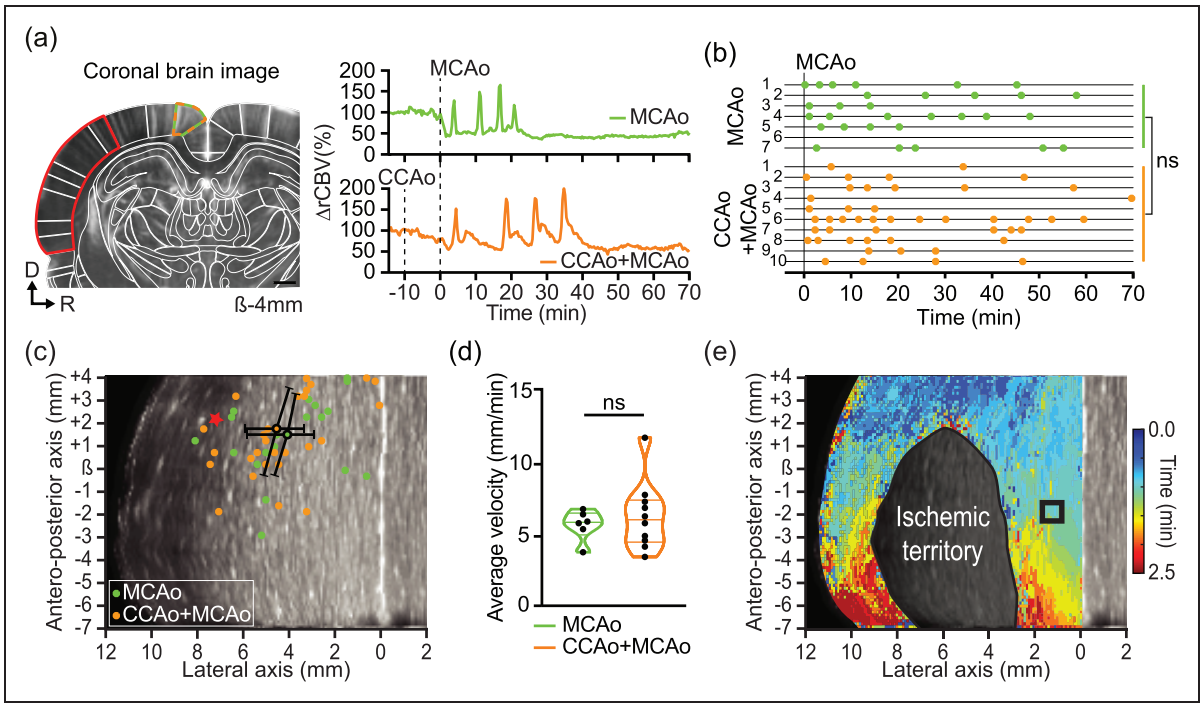

Figure 4. Real-time monitoring of spreading depolarizations using functional ultrasound imaging. (a) A coronal cross-section extracted from the 2D functional ultrasound imaging scan after stroke onset shows the substantial reduction of the rCBV signal in the cortex (red area). The time series plot of the average hemodynamic signal (rCBV) in the retrosplenial granular cortex (green and orange dotted line) from the ischemic hemisphere for each stroke model (MCAo in green; CCAo + MCAo in orange). (b) Monitoring of SDs. Each horizontal line represents one animal; each dot corresponds to the transient hemodynamic increase associated with an SD. The average SDs are not statistically different between the two groups (Unpaired t-test, ns = 0.7557). (c) Location of the epicenter of SDs for the MCAo (green dots) and CCAo + MCAo (orange dots) models with respective centroids (mean ± sd). Red star locates the approximate site of clip placement on the MCA. (d) A plot of the distribution of the average velocity of SDs for MCAo (green) and CCAo + MCAo models (orange). Each point represents one rat. The average SD velocity is not statistically different between the two groups (Unpaired t-test, ns = 0.5683) and (e) Color-coded map showing the propagation of an SD in a concentric manner around the ischemic core from its epicenter located in the anterior part of the brain to the posterior part. D: dorsal, R: right, ß: Bregma reference point. Scale bar: 100 μm.

(Supplementary Figure 5). Single SDs were occurring within the first 5 mins after sham MCAo with rCBV changes and propagation velocity in agreement with the literature. Moreover, no tissue with ischemic damage was observed after the postmortem analysis. It has been reported that the initial SD could be due to the mechanical pressure during the mechanical clipping to occlude the MCA.[37] Excluding this initial SD from our analysis, we observed that the second SD appears rapidly within ~10 mins for both models (MCAo: 6 ± 11 mins, CCAo + MCAo: 11 ± 9 mins). The group analysis of functional ultrasound imaging data for all animals revealed that most SDs were originating from the primary somatosensory cortex (72.2% for MCAo versus 83.3% for CCAo + MCAo) between S1ULp and S1FL (centroid coordinates: ß + 1.5/2 mm, Lateral 4.5/5 mm) in the close vicinity of the area with low rCBV signal (Figure 4(c)). SDs are propagating at a constant velocity. We did not observe differences in the velocity of SDs between MCAo and CCAo + MCAo groups (respectively 5.8 ± 1.0 and 6.4 ± 2.4 mm/min, mean ± sd; p = 0.5683, Unpaired t-test; Figure 4(d)), but the values are in agreement with others studies.[16] All SDs waves observed during this recording period followed a bidirectional propagation from their point of detection, and no cycling SD were observed. Figure 4(e) presents a typical color-coded map overlaid on the unroll cortex projection showing the trajectory and progression of a standard SD from the anterior to the posterior part of the brain by contouring the ischemic territory (Figure 4(e) and Movie 3).

Discussion

We here demonstrate that functional ultrasound imaging is a suitable technology for continuous monitoring of brain-wide hemodynamics during stroke, allowing for real-time assessment of the ischemic insult. We performed repeated 2D brain-wide scans (11 × 12.8 × 9-mm^3

total brain volume) to track the hemodynamics changes from the stroke onset to 70 mins afterward. Anesthetized rats were subjected to either MCAo or CCAo + MCAo stroke model. For each model, we i) characterized the hyper-acute rCBV loss and its spatial extend, ii) tracked individual SDs over the brain, and finally iii) extracted the infarct territories 24 hrs after stroke onset. We show that CCAo + MCAo model provokes a more pronounced and robust ischemia than MCAo alone. Once reconstructed, registered, and segmented on a reference atlas, we observed that infarct territories were more rostral than ischemia, a mismatch that strongly colocalize with the origin of SDs.

We observed that the MCAo and CCAo + MCAo stroke models are significantly different when comparing the volume with a rCBV loss of −100% to −60% relative to baseline level. For such range of rCBV loss, all ischemic regions were exclusively located in the cortex. The volume of tissue progressively decreases from 24 mm^3 5 mins after stroke onset to 15 mm^3 70 mins post-stroke in the MCAo model, an effect that was not observed for the CCAo + MCAo model. This observation is coherent when considering that collateral perfusion is impaired by the ligation of the carotid artery (CCAo). Then, when comparing only the regions with a rCBV loss ranging from −60% to 0%, we showed a slow but continuous perfusion increase following the MCAo in both stroke models. Interestingly, another observation is on the lateral extent of rCBV loss that appears greater after MCAo than CCAo + MCAo; while unexpected, one can suggest that prior CCAo better preserves lateral perfusion.

We quantified the infarct size and found it significantly smaller for the MCAo than for the CCAo + MCAo model despite inter-animal variability in both models, as previously reported for various preclinical stroke models[38] and patients.[39] We observed a significant dispersion of infarct sizes in the CCAo + MCAo even though this model has been shown to provide more robust and reproducible stroke lesions.[23,40,41] Notably, the infarct volume measured at 24 hrs *postmortem* matched those of low rCBV measured *in vivo* using functional ultrasound imaging for the MCAo group but less for the CCAo + MCAo model. For the latter, the infarct size was approximately twice as large when compared with rCBV data, possibly due to reduced collateral flow supporting delayed infarct expansion.[42,43] Hence, brain regions with a significant rCBV loss did not fully overlap with infarct location in both MCAo and MCAo + CCAo model, in accordance to what was previously observed in a context of early partial reperfusion.[14] Indeed, we also showed that the final infarction was located more rostrally as compared to the initial ischemic territory measured 70 mins after stroke for both models.

We demonstrated that the SDs propagate from one point of origin in a rostro-caudal direction with a median velocity of ∼6 mm/min which agrees with range detailed in the literature.[44–48] Interestingly, all SDs originated within brain regions that are not ischemic in the first 70 mins after stroke but turned infarcted at 24 hrs. It is important to note that SDs may occur up to 6 hrs after stroke onset and known to cause an expansion of core-infarcted tissue,[16,49] a period not imaged in our experimental design. Although we did not observe differences in the number of the SDs between the MCAo and CCAo + MCAo stroke during imaging, confirming previous results which demonstrated that the number of SDs was not directly associated with the expansion of the ischemic insult.[46] Finally, our results suggest that the primary somatosensory cortex in rats is highly sensitive to focal brain ischemia and becomes a "hot spot" for generating spreading depolarization, which may contribute to delayed infarction of this region. However, mechanisms and causal effects linking spreading depolarization and the infarct expansion require further investigation.

On the technical limitations of this study, we want to mention the need of large craniotomy, the long anesthesia and the absence of electrophysiology and behavior assessments. Functional ultrasound requires skull opening for imaging deep brain regions[8,27] which may impair both neurological score and infarction size that are indeed significantly improved in rats treated by decompressive craniotomy after MCAo.[50] Therefore, it is likely that our results might underestimate those in close skull since acute ischemia in the MCA territory may lead to cerebral edema with raised intracranial pressure and reduce collateral blood flow, which is associated with larger infarct size.[51] Regarding the prolonged anesthesia along surgery and imaging, it has a direct impact on the cerebral blood flow, neurovascular coupling, autoregulation, ischemic depolarizations, excitotoxicity, inflammation, neural networks, and numerous molecular pathways relevant for stroke outcome.[52–58] It is important to note that our study was not specifically designed to record brain hemodynamics after the recovery from anesthesia. However, it is worth mentioning that recent advances in the field, particularly in awake stroke research, provide promising opportunities to overcome this limitation.

Additionally, we did not record the neuronal activity of the ischemic core or peri-ischemic territory to confirm that rCBV signal is associated with electrical SD. However, functional ultrasound imaging signal has been repeatedly validated as a robust and trustable proxy of the neural activity using electrophysiological recording[8,59–61] or calcium imaging,[62] and also suited for tracking with high reliability propagating seizures.[9] Moreover, several studies have already demonstrated

the direct link between hemodynamic and neuronal signals in ischemia[63,64] and spreading depolarization context.[22,35,65] Finally, it is important to note that we did not specifically investigate the impact of sex dimorphism on the ischemic insult[66] or early behavioral outcomes following the insult, as recommended by the STAIR guidelines for enhancing the translational value of preclinical stroke research.[67]

The recent development toward imaging brain-wide hemodynamics in awake rodents[26] combined with experimental model to induce stroke in conscious rodents[68] will support future investigation on the link between ischemia, SD and infarction expansion.

Funding

The author(s) disclosed receipt of the following financial support for the research, authorship, and/or publication of this article: This work is supported by grants from the Fondation Leducq (15CVD02) and KU Leuven (C14/18/099-STYMULATE-STROKE). The functional ultrasound imaging platform is supported by grants from FWO (MEDI-RESCU2-AKUL/17/049, G091719N, and 1197818 N), VIB Tech-Watch (fUSI-MICE), Neuro-Electronics Research Flanders TechDev fund (3D-fUSI project). The Endres lab received funding from DFG under Germany's Excellence Strategy – EXC-2049 – 390688087, BMBF, DZNE, DZHK, EU, Corona Foundation, and Fondation Leducq

Acknowledgements

The authors thank all the members of the Fondation Leducq network #15CVD02 for helpful comments and discussions. We thank all NERF animal caretakers, including I. Eyckmans, F. Ooms, and S. Luijten, for their help with the management of the animals.

Declaration of conflicting interests

The author(s) declared the following potential conflicts of interest with respect to the research, authorship, and/or publication of this article: A.U. is the founder and a shareholder of AUTC company commercializing functional ultrasound imaging solutions for preclinical and clinical research.

Authors' contributions

Study conception and methodology were performed by CB, NLD, KG, ME, and AU. Software was designed by GM and AU. Imaging acquisition was designed by CB, GM, AU, and data collection was performed CB. Histochemistry was performed by NLD and MG. Data analysis and interpretation were performed by CB, NLD, GM, and AU. CB wrote the first draft of the manuscript which was further edited by NLD, GM, ME, and AU. All authors (CB, NLD, KG, MG, GM, ME, and AU) read, commented on, and approved the final manuscript. Study funding (ME, AU), set-up (CB, GM), supervision (KG, GM, ME, AU), responsibility for the data (AU).

ORCID iD

Clément Brunner https://orcid.org/0000-0002-2567-4832

Supplementary material

Supplemental material for this article is available online.

References

1. Astrup J, Siesjö BK and Symon L. Thresholds in cerebral ischemia – the ischemic penumbra. *Stroke* 1981; 12: 723–725.
2. Maas MB, Lev MH, Ay H, et al. Collateral vessels on CT angiography predict outcome in acute ischemic stroke. *Stroke* 2009; 40: 3001–3005.
3. Saver JL. Time is brain–quantified. *Stroke* 2006; 37: 263–266.
4. Martín A, Ramos-Cabrer P and Planas AM. Noninvasive brain imaging in small animal stroke models: MRI, PET, and SPECT. In: *Neuromethods*. New York: Springer, 2016, pp.147–186.
5. Baron J-C. Recent advances in mesoscopic-scale imaging in animal models of ischemic stroke. *Curr Opin Neurol* 2016; 29: 104–111.
6. Urban A, Golgher L, Brunner C, et al. Understanding the neurovascular unit at multiple scales: advantages and limitations of multi-photon and functional ultrasound imaging. *Adv Drug Deliv Rev* 2017; 119: 73–100.
7. Markicevic M, Savvateev I, Grimm C, et al. Emerging imaging methods to study whole-brain function in rodent models. *Transl Psychiatry* 2021; 11: 457.
8. Urban A, Mace E, Brunner C, et al. Chronic assessment of cerebral hemodynamics during rat forepaw electrical stimulation using functional ultrasound imaging. *Neuroimage* 2014; 101: 138–149.
9. Macé E, Montaldo G, Cohen I, et al. Functional ultrasound imaging of the brain. *Nat Methods* 2011; 8: 662–664.
10. Macé E, Montaldo G, Osmanski B-F, et al. Functional ultrasound imaging of the brain: theory and basic principles. *IEEE Trans Ultrason Ferroelectr Freq Control* 2013; 60: 492–506.
11. Montaldo G, Urban A and Macé E. Functional ultrasound neuroimaging. *Annu Rev Neurosci* 2022; 45: 491–513.
12. Brunner C, Isabel C, Martin A, et al. Mapping the dynamics of brain perfusion using functional ultrasound in a rat model of transient Middle cerebral artery occlusion. *J Cereb Blood Flow Metab* 2017; 37: 263–276.
13. Brunner C, Korostelev M, Raja S, et al. Evidence from functional ultrasound imaging of enhanced contralesional microvascular response to somatosensory stimulation in acute middle cerebral artery occlusion/reperfusion in rats: a marker of ultra-early network reorganization? *J Cereb Blood Flow Metab* 2018; 38: 1690–1700.
14. Hingot V, Brodin C, Lebrun F, et al. Early ultrafast ultrasound imaging of cerebral perfusion correlates with ischemic stroke outcomes and responses to treatment in mice. *Theranostics* 2020; 10: 7480–7491.

15. Dreier JP. The role of spreading depression, spreading depolarization and spreading ischemia in neurological disease. *Nat Med* 2011; 17: 439–447.
16. Ayata C and Lauritzen M. Spreading depression, spreading depolarizations, and the cerebral vasculature. *Physiol Rev* 2015; 95: 953–993.
17. Mies G, Iijima T and Hossmann KA. Correlation between peri-infarct DC shifts and ischaemic neuronal damage in rat. *Neuroreport* 1993; 4: 709–711.
18. Busch E, Gyngell ML, Eis M, et al. Potassium-induced cortical spreading depressions during focal cerebral ischemia in rats: contribution to lesion growth assessed by diffusion-weighted NMR and biochemical imaging. *J Cereb Blood Flow Metab* 1996; 16: 1090–1099.
19. Back T, Ginsberg MD, Dietrich WD, et al. Induction of spreading depression in the ischemic hemisphere following experimental middle cerebral artery occlusion: effect on infarct morphology. *J Cereb Blood Flow Metab* 1996; 16: 202–213.
20. Dijkhuizen RM, Beekwilder JP, van der Worp HB, et al. Correlation between tissue depolarizations and damage in focal ischemic rat brain. *Brain Res* 1999; 840: 194–205.
21. von Bornstädt D, Houben T, Seidel JL, et al. Supply-demand mismatch transients in susceptible peri-infarct hot zones explain the origins of spreading injury depolarizations. *Neuron* 2015; 85: 1117–1131.
22. Binder NF, Glück C, Middleham W, et al. Vascular response to spreading depolarization predicts stroke outcome. *Stroke* 2022; 53: 1386–1395.
23. Brint S, Jacewicz M, Kiessling M, et al. Focal brain ischemia in the rat: methods for reproducible neocortical infarction using tandem occlusion of the distal middle cerebral and ipsilateral common carotid arteries. *J Cereb Blood Flow Metab* 1988; 8: 474–485.
24. MacRae I. Preclinical stroke research – advantages and disadvantages of the most common rodent models of focal ischaemia. *Br J Pharmacol* 2011; 164: 1062–1078.
25. Fluri F, Schuhmann MK and Kleinschnitz C. Animal models of ischemic stroke and their application in clinical research. *Drug Des Devel Ther* 2015; 9: 3445–3454.
26. Brunner C, Grillet M, Sans-Dublanc A, et al. A platform for brain-wide volumetric functional ultrasound imaging and analysis of circuit dynamics in awake mice. *Neuron* 2020; 108: 861–875.e7.
27. Brunner C, Grillet M, Urban A, et al. Whole-brain functional ultrasound imaging in awake head-fixed mice. *Nat Protoc* 2021; 16: 3547–3571.
28. Paxinos G. *The rat brain in stereotaxic coordinates*. 6th ed. Amsterdam: Academic Press, 2014.
29. Percie Du Sert N, Hurst V, Ahluwalia A, et al. The ARRIVE guidelines 2.0: updated guidelines for reporting animal research. *PLoS Biol* 2020; 18: e3000410.
30. Wayman C, Duricki DA, Roy LA, et al. Performing permanent distal middle cerebral with common carotid artery occlusion in aged rats to study cortical ischemia with sustained disability. *J Vis Exp* 2016; 108: 53106.
31. ClemBrunner, nerf-common. *Nerf-common/whole-brain-fUS: Whole-brain-fUS*. Zenodo, 2021. doi:10.5281/ZENODO.4905923.
32. Urban A, Brunner C, Dussaux C, et al. Functional ultrasound imaging of cerebral capillaries in rodents and humans. *Jacobs J Mol Transl Med* 2015; 1: 007.
33. ClemBrunner, nerf-common. *nerf-common/whole-brain-fUS: whole-brain-fUS v1.0*. 2021. doi:10.5281/zenodo.4585348.
34. Schindelin J, Arganda-Carreras I, Frise E, et al. Fiji: an open-source platform for biological-image analysis. *Nat Methods* 2012; 9: 676–682.
35. Menyhárt Á, Zölei-Szénási D, Puskás T, et al. Spreading depolarization remarkably exacerbates ischemia-induced tissue acidosis in the young and aged rat brain. *Sci Rep* 2017; 7: 1154.
36. Rabut C, Correia M, Finel V, et al. 4D functional ultrasound imaging of whole-brain activity in rodents. *Nat Methods* 2019; 16: 994–997.
37. Akerman S, Holland PR and Goadsby PJ. Mechanically-induced cortical spreading depression associated regional cerebral blood flow changes are blocked by Na+ ion channel blockade. *Brain Res* 2008; 1229: 27–36.
38. Durand A, Chauveau F, Cho T-H, et al. Spontaneous reperfusion after in situ thromboembolic stroke in mice. *PLoS One* 2012; 7: e50083.
39. Barber PA, Davis SM, Infeld B, et al. Spontaneous reperfusion after ischemic stroke is associated with improved outcome. *Stroke* 1998; 29: 2522–2528.
40. Chen ST, Hsu CY, Hogan EL, et al. A model of focal ischemic stroke in the rat: reproducible extensive cortical infarction. *Stroke* 1986; 17: 738–743.
41. Coert BA, Anderson RE and Meyer FB. Reproducibility of cerebral cortical infarction in the Wistar rat after middle cerebral artery occlusion. *J Stroke Cerebrovasc Dis* 1999; 8: 380–387.
42. Cuccione E, Padovano G, Versace A, et al. Cerebral collateral circulation in experimental ischemic stroke. *Exp Transl Stroke Med* 2016; 8: 2.
43. Beretta S, Versace A, Carone D, et al. Cerebral collateral therapeutics in acute ischemic stroke: a randomized preclinical trial of four modulation strategies. *J Cereb Blood Flow Metab* 2017; 37: 3344–3354.
44. Nakamura H, Strong AJ, Dohmen C, et al. Spreading depolarizations cycle around and enlarge focal ischaemic brain lesions. *Brain* 2010; 133: 1994–2006.
45. Takeda Y, Zhao L, Jacewicz M, et al. Metabolic and perfusion responses to recurrent peri-infarct depolarization during focal ischemia in the spontaneously hypertensive rat: dominant contribution of sporadic CBF decrements to infarct expansion. *J Cereb Blood Flow Metab* 2011; 31: 1863–1873.
46. Bere Z, Obrenovitch TP, Kozák G, et al. Imaging reveals the focal area of spreading depolarizations and a variety of hemodynamic responses in a rat microembolic stroke model. *J Cereb Blood Flow Metab* 2014; 34: 1695–1705.
47. Farkas E, Pratt R, Sengpiel F, et al. Direct, live imaging of cortical spreading depression and anoxic depolarisation using a fluorescent, voltage-sensitive dye. *J Cereb Blood Flow Metab* 2008; 28: 251–262.

48. Bogdanov VB, Middleton NA, Theriot JJ, et al. Susceptibility of primary sensory cortex to spreading depolarizations. *J Neurosci* 2016; 36: 4733–4743.
49. Risher WC, Ard D, Yuan J, et al. Recurrent spontaneous spreading depolarizations facilitate acute dendritic injury in the ischemic penumbra. *J Neurosci* 2010; 30: 9859–9868.
50. Doerfler A, Forsting M, Reith W, et al. Decompressive craniectomy in a rat model of "malignant" cerebral hemispheric stroke: experimental support for an aggressive therapeutic approach. *Foc* 1996; 1: E1.
51. Beard DJ, Logan CL, McLeod DD, et al. Ischemic penumbra as a trigger for intracranial pressure rise – a potential cause for collateral failure and infarct progression? *J Cereb Blood Flow Metab* 2016; 36: 917–927.
52. Newberg LA, Michenfelder JD and Chalon J. Cerebral protection by isoflurane during hypoxemia or ischemia. *Surv Anesthesiol* 1984; 28: 83.
53. Saito R, Graf R, Hübel K, et al. Reduction of infarct volume by halothane: effect on cerebral blood flow or perifocal spreading depression-like depolarizations. *J Cereb Blood Flow Metab* 1997; 17: 857–864.
54. Hartings JA, Rolli ML, Lu X-CM, et al. Delayed secondary phase of peri-infarct depolarizations after focal cerebral ischemia: relation to infarct growth and neuroprotection. *J Neurosci* 2003; 23: 11602–11610.
55. Masamoto K, Fukuda M, Vazquez A, et al. Dose-dependent effect of isoflurane on neurovascular coupling in rat cerebral cortex. *Eur J Neurosci* 2009; 30: 242–250.
56. Seto A, Taylor S, Trudeau D, et al. Induction of ischemic stroke in awake freely moving mice reveals that isoflurane anesthesia can mask the benefits of a neuroprotection therapy. *Front Neuroenergetics* 2014; 6: 1.
57. Kudo K, Zhao L and Nowak TS. Peri-infarct depolarizations during focal ischemia in the awake spontaneously hypertensive rat. Minimizing anesthesia confounds in experimental stroke. *Neuroscience* 2016; 325: 142–152.
58. Hillman TC, Matei N, Tang J, et al. Developing a standardized system of exposure and intervention endpoints for isoflurane in preclinical stroke models. *Med Gas Res* 2019; 9: 46–51.
59. Macé É, Montaldo G, Trenholm S, et al. Whole-brain functional ultrasound imaging reveals brain modules for visuomotor integration. *Neuron* 2018; 100: 1241–1251.e7.
60. Sans-Dublanc A, Chrzanowska A, Reinhard K, et al. Optogenetic fUSI for brain-wide mapping of neural activity mediating collicular-dependent behaviors. *Neuron* 2021; 109: 1888–1905.e10.
61. Nunez-Elizalde AO, Krumin M, Reddy CB, et al. Neural correlates of blood flow measured by ultrasound. *Neuron* 2022; 110: 1631–1640.e4.
62. Aydin AK, Haselden WD, Goulam Houssen Y, et al. Transfer functions linking neural calcium to single voxel functional ultrasound signal. *Nat Commun* 2020; 11: 2954.
63. Weber R, Ramos-Cabrer P, Justicia C, et al. Early prediction of functional recovery after experimental stroke: functional magnetic resonance imaging, electrophysiology, and behavioral testing in rats. *J Neurosci* 2008; 28: 1022–1029.
64. Taylor JM, Zhu X-H, Zhang Y, et al. Dynamic correlations between hemodynamic, metabolic, and neuronal responses to acute whole-brain ischemia. *NMR Biomed* 2015; 28: 1357–1365.
65. Lückl J, Lemale CL, Kola V, et al. The negative ultraslow potential, electrophysiological correlate of infarction in the human cortex. *Brain* 2018; 141: 1734–1752.
66. Bushnell CD, Chaturvedi S, Gage KR, et al. Sex differences in stroke: challenges and opportunities. *J Cereb Blood Flow Metab* 2018; 38: 2179–2191.
67. Fisher M, Feuerstein G, Howells DW, et al. Update of the stroke therapy academic industry roundtable preclinical recommendations. *Stroke* 2009; 40: 2244–2250.
68. Brunner C, Montaldo G and Urban A. Functional ultrasound imaging of stroke in awake rats. 2023. DOI: 10.7554/elife.88919.1.